metals

MDPI

Article

Electrochemical Corrosion Behavior of Fe_3Al/TiC and Fe_3Al-Cr/TiC Coatings Prepared by HVOF in NaCl Solution

Najmeh Ahledel [1], Robert Schulz [2], Mario Gariepy [3], Hendra Hermawan [1] and Houshang Alamdari [1,*]

1 Department of Mining, Metallurgical and Materials Engineering, Université Laval, Québec, QC G1V 0A6, Canada; najmeh.ahledel.1@ulaval.ca (N.A.); hendra.hermawan@gmn.ulaval.ca (H.H.)
2 Hydro-Quebec Research Institute, 1800 Boulevard Lionel Boulet, Varennes, QC J3X 1S1, Canada; Schulz.Robert@ireq.ca
3 Wärtsilä Canada, Inc., American Hydro, 8600 St-Patrick, LaSalle (Montréal), QC H8N 1V1, Canada; mario.gariepy@ahydro.com
* Correspondence: Houshang.Alamdari@gmn.ulaval.ca; Tel.: +1-418-656-7666

Received: 20 December 2018; Accepted: 9 April 2019; Published: 13 April 2019

Abstract: Adding TiC particles into iron aluminide coatings has been found to improve its wear resistance, but its corrosion behavior is less known. In this study, the corrosion behavior of Fe_3Al/TiC and Fe_3Al-Cr/TiC composite coatings, prepared by high velocity oxy fuel (HVOF) spraying, was studied in 3.5 wt. % NaCl solution by means of electrochemical techniques and surface analysis. Results revealed that adding TiC particles into Fe_3Al matrix to improve the wear resistance does not deteriorate the corrosion behavior of Fe_3Al coating. It was also showed that addition of chromium to Fe_3Al/TiC composite provides a more protective layer.

Keywords: corrosion; electrochemical impedance spectroscopy; high velocity oxy fuel coatings; iron aluminide; titanium carbide

1. Introduction

Iron aluminides have received great attention as materials with high potential for a number of industrial applications. This is basically due to their low density, excellent oxidation resistance, hot corrosion resistance, high specific strength and low ductile to brittle transition temperature [1,2]. Their application is, however, limited by their low ductility, poor creep resistance [3] and low wear resistance [4]. It has been shown that the incorporation of ceramic particles into iron aluminide matrix improves its tribological properties [5,6]. For example, the composite coating of iron aluminide with tungsten carbide particles exhibited higher erosive wear-resistance than did the iron aluminide coating alone. Among all ceramic materials, titanium carbide (TiC), owing to its excellent mechanical, chemical and thermal properties, has been identified as a good reinforcing phase to improve the mechanical properties of the aluminide matrix [7,8]. Chen et al. [9] noted that Fe-Al intermetallics with TiC reinforcement have excellent dry sliding wear resistance. In addition to laser cladding, several other techniques, such as plasma spraying [10–13], wire arc spraying [14] and high-velocity oxy-fuel (HVOF) projection [15] have also been used to deposit Fe-Al alloys on carbon steels or stainless steel substrates. HVOF is a convenient process to deposit thick coatings on variety of substrates with superior properties at low cost [16]. The process utilizes a combination of oxygen with various fuel gases including hydrogen, propane, propylene and kerosene as the feed of the combustion chamber while the spray powder (mixed metal or oxides) comes through from other side. The combustion of the gases provides the temperature and pressure needed to flow the gases through the nozzle. With the flame temperature

ranging between 2500 and 3200 °C, powder particles partially or completely melt during the flight through the nozzle and due to the presence of oxygen and high temperature, oxidation also occurs.

Although iron aluminides are mainly developed for applications at high temperatures, they also exhibit a high potential for low-temperature applications. These intermetallics are good candidates to replace stainless steel in several applications, i.e., pipes and tubes for heating elements and main components for distillation and desalination plants [17]. A number of studies were thus concentrated on the aqueous corrosion behavior of these materials to test their durability in various corrosive environments. The corrosion behavior of iron aluminides has been studied in several acidic and basic solutions [18–24]. Chiang et al. [18] evaluated the passivation behavior of Fe-Al alloys containing 3.4, 10.4, 18.7, 19.4, 29.5, and 41.7 at. % Al. They showed that Fe-Al alloys, with an Al content exceeding 19 at. %, have wide passivation regions and low passivation current in 0.1 N H_2SO_4. In addition, when the Al content of Fe-Al alloys exceeds this limit, further increment of Al content has only a slight influence on passivation. Sharma et al. [19] compared the stability of the passive film and pitting behavior of Fe-28Al (at. %) and Fe-28Al-3Cr (at. %) with AISI SS 304 under different pH conditions to evaluate their performance in acidic, basic, and neutral solutions. They reported that the presence of 3 at. % Cr in iron aluminides improves their aqueous corrosion resistance and makes them comparable to AISI SS 304. Porcayo-Calderon et al. [20] studied corrosion behavior of FeAl and Fe_3Al coatings prepared by two thermal spray techniques, flame spraying and HVOF using three different particle sizes and compared their corrosion behavior with that of the base alloys in 1.0 M NaOH solution at room temperature. The coatings prepared using medium particle size and flame spray and those using fine particle size and HVOF spray were shown to be more stable, uniform, denser, and with lower porosity, thus exhibited a greater corrosion resistance. Grosdidier et al. [21] prepared nanocrystalline Fe-40Al coatings by HVOF with varied amount of hard un-melted particles of feedstock powder and found that feedstock powder size has a strong effect on the coating hardness. The electrochemical response of the coatings revealed that these particles were the reason of poor corrosion resistance compared to bulk material. Analysis of corrosion damage showed a prevalent localized attack at intersplat boundaries or around un-melted powder particles, probably enhanced by galvanic phenomena. Amiriyan et al. [4,25] reported that the Vickers hardness and the dry sliding wear resistance of Fe_3Al/TiC composite coatings, at sliding speeds ranging from 0.04 to 0.8 $m \cdot s^{-1}$ and under a constant load of 5 N, increased as the amount of TiC particles in Fe_3Al matrix increased. They also compared the phase composition, microstructure, micro hardness and elastic modulus of Fe_3Al and Fe_3Al/TiC composite coatings, however the authors did not report the corrosion behavior of these coatings. Related to corrosion behavior, Rao [23] proposed a mechanistic model for re-passivation of iron aluminide in comparison to pure Al and Fe, based on his investigation using a rapid scratched electrode technique in 0.25 M H_2SO_4.

Both the mechanical or electrochemical properties of Fe-Al intermetallics can be improved by alloying elements in the form of solid solutions [26–30]. The addition of 6 at. % Cr improved the ductility of Fe_3Al up to 10% [31]. A few mechanisms were proposed to explain the effect of Cr on mechanical and corrosion properties of Fe_3Al. First, it has been postulated that Cr in solid solution facilitates the dislocation cross-slipping and solid solution softening [32,33]. Epelboin et al. [34] also showed that Cr affects the surface properties through the contribution of chromium oxides to the formation of passive layers and the decrement of reaction kinetics. The decrease of water reduction reaction rate may also lead to the reduction of hydrogen evolution and thus mitigating the hydrogen embrittlement [35].

In this work, we studied the corrosion behavior of Fe_3Al/TiC composite coatings, prepared by HVOF technique. These coatings had shown improved wear resistance [4,25] however, their corrosion behavior had not been reported. The effect of Cr on the passivity of Fe_3Al/TiC composite in 3.5 wt. % NaCl solution was revealed.

2. Materials and Methods

2.1. Coating Preparation

The starting materials in powder form were prepared by mechanically alloying commercial iron aluminide (Fe_3Al, 96% purity), titanium (Ti, 99.4% purity) and chromium (Cr, 99% purity) (Alfa Aesar, Haverhill, MA, USA), and graphite (C, 96% purity, Asbury Graphite Mills, Asbury, NJ, USA). The nominal composition of the feedstock powder before milling is given in Table 1.

Table 1. Nominal composition of the feedstock powder before milling.

Sample	at. % of Elements				
	Fe	Al	Ti	C	Cr
Fe_3Al	75	25	0	0	0
Fe_3Al/TiC	50	16.66	16.66	16.66	0
Fe_3Al-Cr/TiC	37.5	12.5	12.5	12.5	25

A 300 g batch of each powder mixture was placed in a high-energy ball mill (Zoz GmbH, Wenden, Germany, Simoloyer CM08) and milled under argon atmosphere for 6 h. Hardened steel balls (52100 heat-treated steel with a hardness of 60–64 Rockwell C) and jar were used and a ball to powder weight ratio of 10:1 was chosen for milling. The XRD patterns of the milled powder, were provided in other work by Amiriyan et al. [4,25]. The milled powders were then heat-treated at 1000 °C for 2 h under 10^{-6} mbar of vacuum. This post-treatment was performed in order to ensure the maximum reaction between the additive elements. In fact, the ball milling provides a mixture with a good homogeneity and the reaction between additive elements starts during milling. However, to complete these reactions, very long milling times are required. The post-treatment at 1000 °C helps the completion of these reactions. Based on the X-Ray diffraction patterns, the peaks related to the additive elements are disappeared after this post treatment. Titanium carbide starts forming by mechano-chemical reaction between titanium and graphite during milling and this reaction progresses during the subsequent heat treatment and the final product is a composite of Fe_3Al matrix and TiC particles [4]. The composite powders were deposited on mild steel plates (AISI 1020) using a JP-8000 HVOF spray system (Praxair Surface Technologies, Indianapolis, IN, USA) with spray parameters listed in Table 2. The substrates were sand-blasted and then washed with acetone and ethanol prior to HVOF deposition. Argon and kerosene were used as the carrier gas and the fuel during the HVOF deposition, respectively. A coating with 150–200 micron thickness was deposited on the substrate. Coated samples were rinsed with ethanol before corrosion test and no polishing was performed.

Table 2. High-velocity oxy-fuel (HVOF) spraying parameters.

Oxygen flow rate (m^3/s)	1.5×10^{-2}
Kerosene flow rate (m^3/s)	5.57×10^{-6}
Carrier gas	Argon
Spraying distance (m)	0.38
Number of deposition passes	5

2.2. Electrochemical Tests

The open circuit potential (OCP) and potentiodynamic polarization tests were carried out using a VersaSTAT3 Potentiostat (Ametek Princeton Applied Research, Oak Ridge, TN, USA) in a conventional three-electrode cell. A Princeton model K0235 flat cell, accommodating wide range of electrode shapes and sizes, was used in order to test different areas of a similar sample without cutting it. An Ag/AgCl was used as reference electrode and a platinum mesh as a counter electrode. All tests were performed in an electrolyte containing 3.5 wt. % NaCl with magnetic stirring at 60 rpm at room temperature

(25 ± 2 °C). The OCP was measured over 20 h of immersion. Potentiodynamic polarization was conducted from −0.7 to +2 V with respect to the OCP, using a scanning rate of 1 mV/s. Before starting the experiments, the electrodes were left for one hour in the solution to stabilize at their free corrosion potential. The surface of samples were washed with ethanol before testing. All experiments were repeated three times.

Electrochemical impedance spectroscopy (EIS) was carried out using a Reference 3000 potentiostat/galvanostat (Gamry Instruments, Warminster, PA, USA). Electrodes were mounted in epoxy resin and assembled in a three-electrode teflon holder. A platinum foil with a surface of 1 cm^2 was used as cathode and an Ag/AgCl (KCl sat.) as the reference electrode. Prior to EIS experiments, one-hour stabilization time was considered then the frequency scanning was performed from 10^{-2} to 10^5 Hz with a root-mean square potential amplitude of 5 mV. The interpretation of EIS results was made with the help of ZSimpWin software (Ametek Princeton Applied Research, Oak Ridge, TN, USA).

2.3. Surface Analysis

The cross-sectional morphology of the coatings was studied after performing the potentiodynamic polarization tests by using a scanning electron microscope (SEM, JSM-840A, JEOL Inc., Peabody, MA, USA) equipped with an energy dispersive X-ray spectroscopy (EDS, SwiftED 3000, Oxford Instruments, Concord, MA, USA). Further surface chemistry analysis was performed by using an X-ray photoelectron spectroscopy (XPS, Axis-Ultra, Kratos Analytical, Manchester, UK), using an incident X-ray radiation of Al Kα under vacuum (10^{-12} bar). The surface film was analyzed at a take-off angle of 30°. Narrow multiple scans were recorded with 160 and 1 eV step sizes. High resolution spectra were recorded at pass energies of 40 and 20 eV and step sizes of 0.1 and 0.05 eV. Apparent relative concentrations were calculated using the CasaXPS software (Casa Software, Teignmouth, UK) with the appropriate sensitivity factors.

3. Results and Discussion

3.1. Electrochemical Behavior

The variation of OCP of metallic materials as a function of time gives valuable information about film formation and passivation. A rise of potential in the positive direction indicates the formation of a protective film, a steady potential indicates the presence of an intact and protective film, and a drop of potential in the negative direction indicates breakage or dissolution of the film, or no film formation at all [36]. The OCP vs Ag/AgCl reference electrode plots of all tested coatings (Figure 1a) show that at the early moments of immersion the potential rapidly shifts towards negative, indicating the dissolution of the oxide layer existing before immersion. The potential then experienced a steady state and no change was observed until the end of the experiment over 20 h, indicating an equilibrium established between the corrosion and the formation of an oxide film on the surface. The Fe_3Al coating exhibited more negative potential value than did of Fe_3Al/TiC and Fe_3Al-Cr/TiC coatings. Adding TiC shifted the absolute potential of Fe_3Al to less negative value. This indicates that for composite coatings, corrosion via dissolving the electrode surface decreased.

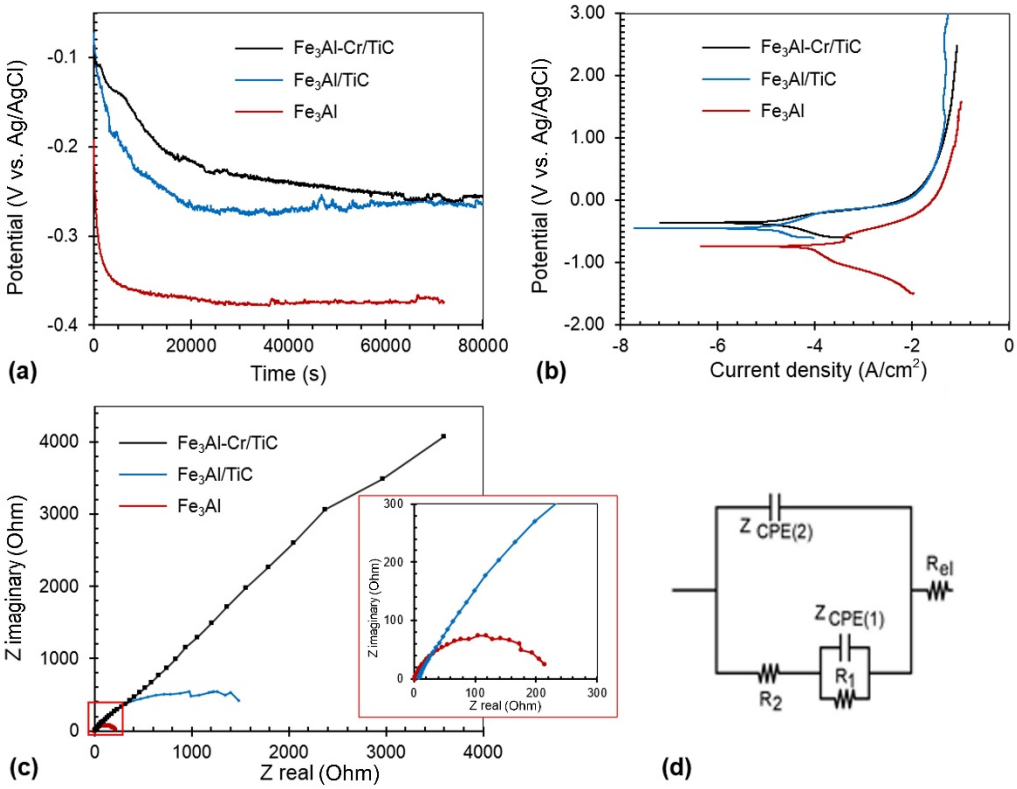

Figure 1. Electrochemical test results of Fe_3Al, Fe_3Al/TiC and Fe_3Al-Cr/TiC in freely aerated 3.5 wt. % NaCl solution: (**a**) open circuit potential measured for up to 20 h, (**b**) potentiodynamic polarization curves, (**c**) Nyquist plots, and (**d**) proposed equivalent circuit model.

The three coatings show a similar shape of polarization curves (Figure 1b). A difference is observed as the composite coatings (Fe_3Al/TiC and Fe_3Al-Cr/TiC) show a nobler corrosion potential (E_{corr}) and a lower corrosion current density (j_{corr}) than that of the Fe_3Al. This observation is in accordance with the OCP results. Although the current density remains constant beyond a certain potential range, the curves do not demonstrate an active-passive behavior, and no breakdown potential can be observed even at relatively high potentials. The values of corrosion parameters obtained from the polarization curve, such as cathodic Tafel (β_c) and anodic Tafel (β_a) slopes, and polarization resistance (R_p) are presented in Table 3. The results indicate that adding TiC particles to Fe_3Al matrix decreases the anodic and cathodic current density and the value of E_{corr} shifts to the less negative direction. In composite coatings, smaller values of j_{corr} and greater amounts of R_p compared to Fe_3Al, revealed that the corrosion performance of composite coatings in 3.5% NaCl solution has been improved by adding TiC. A decrease of calculated corrosion rate (*CR*) is also shown by the composite coating which further decreasing by the addition of Cr into the Fe_3Al/TiC.

Table 3. Corrosion parameters obtained from the polarization curves.

Sample	β_c (mV·dec^{-1})	E_{corr} (mV)	β_a (mV·dec^{-1})	j_{corr} (μA·cm^{-2})	R_p (Ω·cm^2)	*CR* (mm·y^{-1})
Fe_3Al	350	−780	250	83.8	15.3	7.7×10^{-9}
Fe_3Al/TiC	380	−480	380	13.9	300	1.4×10^{-9}
Fe_3Al-Cr/TiC	170	−350	250	9.9	205	0.4×10^{-9}

The electrochemical impedance spectroscopy (EIS) test results, represented in the form of Nyquist plots (Figure 1c), show two types of diagrams. The first type, as also shown in magnified inset of (Figure 1c) is related to Fe_3Al and Fe_3Al/TiC samples and consists of two overlapped capacitive loops. The time constant at high frequencies is attributed to the corrosion product layer while the second at

intermediate and low frequencies is ascribed to the faradaic charge transfer process [37]. Compared to Fe_3Al, the composite coatings exhibit higher impedance values, indicating that the corrosion products layer formed on the surface is more protective than that formed on Fe_3Al [38]. This result is in good agreement with the results obtained by potentiodynamic tests. The second type (the black curve in the main diagram of Figure 1c) is related to Fe_3Al-Cr/TiC showing a much larger diameter of the arc, indicating larger impedance due to the addition of Cr into Fe_3Al/TiC. The diagram consists of a small semicircle, tended to be a straight line with a slope of around 45° (after Z_{real} = 500). Since a slope higher than 45° was reported to be the characteristic of a diffusion process, corresponding to a concentration gradient localized in a porous layer and in the solution [38], this response for Fe_3Al-Cr/TiC could therefore be the characteristic of a diffusion process while the semicircle curves of Fe_3Al and Fe_3Al/TiC are attributed to a charge transfer process. In order to provide quantitative support to the experimental EIS results, an equivalent circuit was proposed (Figure 1d) and the related impedance parameters were fitted and calculated (Table 4).

Table 4. Impedance fitting parameters.

Sample	R_{el} ($\Omega\cdot cm^2$)	R_2 ($\Omega\cdot cm^2$)	(CPE_2) Y_{02} ($S\cdot cm^{-2}\cdot s^n$)	n_2	R_1 ($\Omega\cdot cm^2$)	(CPE_1) Y_{01} ($S\cdot cm^{-2}\cdot s^n$)	n_1
Fe_3Al	1.9	187.3	7.9×10^{-3}	0.8	27.7	70×10^{-3}	1
Fe_3Al-TiC	1.8	402.1	4.2×10^{-3}	0.68	160	4.7×10^{-3}	0.6
Fe_3Al-Cr/TiC	7.2	1979	8.7×10^{-6}	0.9	16.8×10^3	0.8×10^{-3}	0.8

In the proposed equivalent circuit model, R_{el} corresponds to the resistance of the electrolyte while R_2 and CPE_2 represent the resistance and the capacitance of the corrosion product layer, respectively. R_1 represents the charge transfer resistance, and CPE_1 represents the double-layer capacitance. A constant phase element (*CPE*) was used to consider a deviation from an ideal capacitor. The origins of the *CPE* were summarized by Jorcin et al. [39], which includes distributed surface roughness and heterogeneity, slow adsorption reaction, non-uniform potential and current distribution. CPE_1 and CPE_2 are two constant phase elements of the equivalent circuit and n_1 and n_2 are corresponding exponents ($CPE = Y_0(j\omega)^n$). *CPE* can represent pure resistance ($n = 0$), pure capacitance ($n = 1$), Warburg impedance ($n = 0.5$) or inductance ($n = -1$) [28]. The calculated parameters indicate that the values of fractional exponent, n_2, for all specimens are close to 1, being near to that of a pure capacitance. The CPE_2 possesses physical meaning of the capacitance of the corrosion products layer ($C = \varepsilon_r\, \varepsilon_0 \frac{A}{d}$) that is inversely proportional to the thickness of the corrosion layer (d).

The CPE_2 values for composite coatings (Fe_3Al/TiC and Fe_3Al-Cr/TiC) are less than that of Fe_3Al. This result could be due to an increase of the thickness of the corrosion product layer or its composition change. R_2 value is also higher for the composite samples, compared to the pure Fe_3Al. This value significantly increases by adding Cr into the composite. The increase of the resistance of the corrosion products layer, R_2, for composite coatings indicates that the layer is more resistant to electron transfer. This could be an indication of the compactness of this layer, i.e., more compact corrosion product layer can block the dissolution reaction, providing an effective barrier against corrosion. Therefore, among the composite samples, the corrosion product resistance of Fe_3Al-Cr/TiC is much greater than that of Fe_3Al/TiC. The charge transfer resistance, R_1 of Fe_3Al/TiC is also higher than that of the two other samples, which is likely due to the blocking effect of the more compact corrosion product layer formed at the surface. R_1 for composite coatings (Fe_3Al/TiC and Fe_3Al-Cr/TiC) are considerably higher than that of Fe_3Al.

3.2. Surface Analysis

After potentiodynamic polarization test, three distinct layers are observed on the cross-section of the tested samples, i.e., substrate, coating and corrosion products (Figure 2). A thick layer of corrosion product uniformly covered the entire surface of the coatings. The coating consists of lamellar

microstructure. This structure is typical in the HVOF process while partially molten particles hit the surface of the substrate and spread on, resulting in a lamellar microstructure called splats, which appears in the form of elongated grains at the cross-section view.

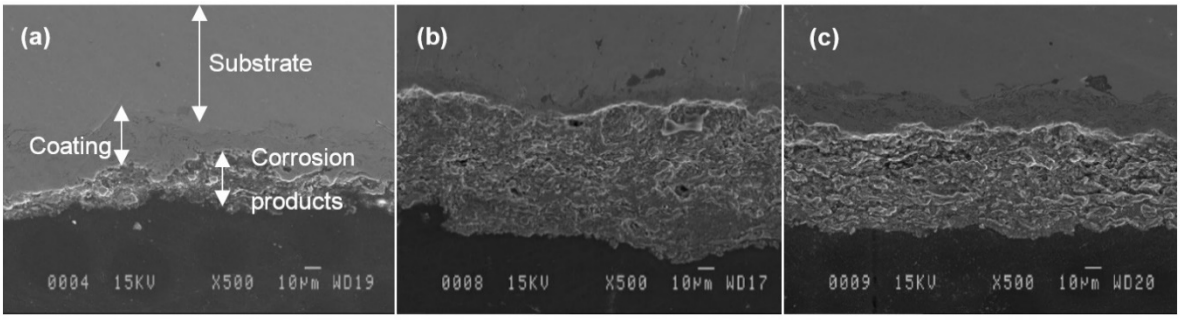

Figure 2. Cross-sectional SEM micrograph of the corrosion product layer formed on: (**a**) Fe_3Al, (**b**) Fe_3Al/TiC, and (**c**) Fe_3Al-Cr/TiC after subjected to the potentiodynamic polarization test.

The XPS analysis results confirm the presence of a mixture of FeO and Fe_2O_3 as well as Al_2O_3 on the top layer of all three coatings (Figures S1 and S2a, Supplementary File). Other detected corrosion products are Al_2O_3, $Al(OH)_3$ and $AlCl_3$ (Figure S2, Supplementary File). The oxides could be formed during HVOF process, similar to that reported by Frangini et al. [13]. They reported that the outer part of the oxide layer predominantly consists of mixed Al-Fe oxy-hydroxide whereas the inner part is of mostly an Al-rich oxide phase. The hydroxides and chlorides are formed during polarization tests due to the presence of sodium chloride in the solution. On the XPS spectra of the two composite coatings appear also the peaks associated with TiO, TiO_2 and $Cr(OH)_3$ (Figure S3, Supplementary File). These results as well as the EDS analysis of the corrosion products indicate that a corrosion product layer was formed on the composite coatings (Fe_3Al/TiC and Fe_3Al-Cr/TiC) and consists of a mixture of aluminum, iron and titanium oxide, aluminum hydroxide, titanium carbide and chromium hydroxide in case of Fe_3Al-Cr/TiC. The presence of hydroxide could be the result of hydration of product film that can happen by raising potential, as reported by Rao [23]. The elemental analysis, extracted from XPS spectra of the three coatings before and after polarization tests, reveals the composition of the top oxide layer (Table 5). In addition to the elements presented in Table 5, an appreciable amount of carbon and oxygen was also detected by XPS analysis. Oxygen in coatings before the test could be due to the oxidation of the feedstock during coating by HVOF technique or to the natural oxidation in contact with air. The presence of carbon is due to TiC. However, carbon is also present in the sample without TiC. One source of carbon and oxygen, detected by XPS, is usually the chemisorption of CO and CO_2 on the sample. The amount of the chemisorbed species could be significant on the porous materials with high surface area. As it is difficult to quantify the portion of analyzed carbon and oxygen coming from the chemisorption, the XPS data in Table 5 were presented only for the elements other than oxygen and carbon. Therefore, the at. % in this table is the relative amount of each element normalized on the sum of the analyzed elements (i.e., Fe, Al, Ti, Cr, Cl).

Table 5. XPS surface analysis of the samples (excluding carbon and oxygen) before and after polarization tests. The at. % is the normalized value for each element on the sum of all elements presented in the table.

at. %	Fe_3Al		Fe_3Al/TiC		Fe_3Al-Cr/TiC	
	Before Test	After Corrosion	Before Test	After Corrosion	Before Test	After Corrosion
Fe	62	22	54	31	36	29
Al	37	67	34	14	30	6.8
Ti	0.0	0.0	10	37	11	32
Cr	1.1	1	1.7	8.5	23	20
Cl	0.0	9.8	0.0	8.7	0.0	11

A notable increase of Al content is detected on Fe_3Al coating after corrosion, but not on the two composite coatings. Rao [23] stated that Al gets enriched on the surface of Fe_3Al coating due to the formation of oxide and chloride, whereas Fe gradually dissolves into the corrosive solution of H_2SO_4. A significant increase of Ti content is detected on both composite coatings, which could be related to the formation of TiO_2 and accumulation of TiC in the corrosion products. In addition, sample Fe_3Al-Cr/TiC exhibits a large amount of Cr in the corrosion products. As discussed by Zamanzade et al. [40], Cr^{3+} may substitute the Al^{3+} sites during the formation of the passive film by diffusion into the solution/oxide interface.

4. Conclusions

Adding TiC into Fe_3Al matrix, prepared by high-velocity oxy-fuel spraying, increases the corrosion resistance of Fe_3Al/TiC composite coating in 3.5 wt. % NaCl solution. The corrosion rates of Fe_3Al/TiC coating are about five times lower than that of Fe_3Al. The addition of Cr into Fe_3Al/TiC further decreases the corrosion rate of Fe_3Al-Cr/TiC coating to three times lower than that of Fe_3Al/TiC. A corrosion product layer consisting of a mixture of aluminum, iron and titanium oxide and aluminum hydroxide is formed on the samples. Chromium hydroxide as also formed in case of Fe_3Al-Cr/TiC. A more compact corrosion layer formed on the Fe_3Al-Cr/TiC leads to a corrosion mechanism via diffusion process, while the Fe_3Al/TiC and Fe_3Al corrode via a charge transfer mechanism. Finally, this work concludes that the benefit of adding TiC particles into Fe_3Al matrix to improve the wear resistance does not deteriorate its corrosion resistance, and further addition of Cr slightly improves its corrosion resistance even more.

Supplementary Materials: The following are available online at http://www.mdpi.com/2075-4701/9/4/437/s1, Figure S1: XPS spectra for Fe2p for: (**a**) Fe_3Al, (**b**) Fe_3Al/TiC, and (**c**) Fe_3Al-Cr/TiC, Figure S2: XPS spectra of Al2p for Fe_3Al/TiC: (**a**) before and (**b**) after polarization test, Figure S3: XPS spectra of Ti2p for: (**a**) Fe_3Al/TiC (**b**) Fe_3Al-Cr/TiC, and (**c**) Cr2p of Fe_3Al-Cr/TiC.

Author Contributions: N.A. conducted the research under the supervision of H.A. and H.H. R.S. and M.G. contributed in design of the experiments and result analysis during the research activities.

Funding: Natural Sciences and Engineering Research Council of Canada (NSERC) via the Discovery Grant.

Acknowledgments: The authors would like to acknowledge the financial support of Natural Sciences and Engineering Research Council of Canada, Fonds de Recherche du Québec-Nature et Technologies, and the Aluminum Research Centre–REGAL. The assistance of Silvio Savoie (Hydro-Quebec Research Institute, Montreal, QC, Canada) and Guillaume Gauvin (Université Laval) for conducting HVOF depositions and the chemical analyses is also gratefully acknowledged.

Conflicts of Interest: The authors declare no conflict of interest.

References

1. Rao, V.S. A review of the electrochemical corrosion behavior of iron aluminides. *Electrochim. Acta* **2004**, *49*, 4533–4542. [CrossRef]
2. Zamanzade, M.; Barnoush, A.; Motz, C. A review on the properties of iron aluminide intermetallics. *Crystals* **2016**, *6*, 10. [CrossRef]
3. Cinca, N.; Lima, C.R.C.; Guilemany, J.M. An overview of intermetallics research and application: Status of thermal spray coatings. *J. Mater. Res. Technol.* **2013**, *2*, 75–86. [CrossRef]
4. Amiriyan, M.; Alamdari, H.; Blais, C.; Savoie, S.; Schulz, R.; Gariépy, M. Dry sliding wear behavior of Fe_3Al and Fe_3Al/TiC coatings prepared by HVOF. *Wear* **2015**, *342*, 154–162. [CrossRef]
5. Xu, B.; Zhu, Z.; Ma, S.; Zhang, W.; Liu, W. Sliding wear behavior of Fe–Al and Fe–Al/WC coatings prepared by high velocity arc spraying. *Wear* **2004**, *257*, 1089–1095. [CrossRef]
6. Zhu, Z.-X.; Liu, Y.; Xu, B.-S.; Ma, S.-N.; Zhang, W. Influence of heat treatment on microstructure and wear behavior of Fe-Al/WC composite coatings. *J. Mater. Eng.* **2004**, *7*, 3–5.
7. Durlu, N. Titanium carbide based composites for high temperature applications. *J. Eur. Ceram. Soc.* **1999**, *19*, 2415–2419. [CrossRef]
8. Hussainova, I. Some aspects of solid particle erosion of cermets. *Tribol. Int.* **2001**, *34*, 89–93. [CrossRef]

9. Chen, Y.; Wang, H. Microstructure and wear resistance of laser clad TiC reinforced FeAl intermetallic matrix composite coatings. *Surf. Coat. Technol.* **2003**, *168*, 30–36. [CrossRef]
10. Kumar, S.; Selvarajan, V.; Padmanabhan, P.V.A.; Sreekumar, K.P. Characterization and comparison between ball milled and plasma processed iron-aluminium thermal spray coatings. *Surf. Coat. Technol.* **2006**, *201*, 1267–1275. [CrossRef]
11. Song, B.; Dong, S.; Coddet, P.; Hansz, B.; Grosdidier, T.; Liao, H.; Coddet, C. Oxidation control of atmospheric plasma sprayed Fe-Al intermetallic coatings using dry-ice blasting. *J. Therm. Spray Technol.* **2013**, *22*, 345–351. [CrossRef]
12. Luer, K.R.; DuPont, J.N.; Marder, A.R. High-Temperature sulfidation of Fe_3Al thermal spray coatings at 600 °C. *Corrosion* **2000**, *56*, 189–198. [CrossRef]
13. Frangini, S.; Masci, A. Intermetallic FeAl based coatings deposited by the electrospark technique: Corrosion behavior in molten (Li+K) carbonate. *Surf. Coat. Technol.* **2004**, *184*, 31–39. [CrossRef]
14. Pokhmurska, H.; Dovhunyk, V.; Student, M.; Bielanska, E.; Beltowska, E. Tribological properties of arc sprayed coatings obtained from FeCrB and FeCr-based powder wires. *Surf. Coat. Technol.* **2002**, *151–152*, 490–494. [CrossRef]
15. Szczucka-Lasota, B.; Formanek, B.; Hernas, A.; Szymanski, K. Oxidation models of the growth of corrosion products on the intermetallic coatings strengthened by a fine dispersive Al_2O_3. *J. Mater. Proc. Technol.* **2005**, *164–165*, 935–939. [CrossRef]
16. Sidhu, T.; Prakash, S.; Agrawal, R. Studies on the properties of high-velocity oxy-fuel thermal spray coatings for higher temperature applications. *Mater. Sci.* **2005**, *41*, 805–823. [CrossRef]
17. Rosalbino, F.; Carlini, R.; Parodi, R.; Zanicchi, G. Effect of silicon and germanium alloying additions on the passivation characteristics of Fe_3Al intermetallic in sulphuric acid solution. *Electrochim. Acta* **2012**, *62*, 305–312. [CrossRef]
18. Chiang, W.-C.; Luu, W.-C.; Wu, J.-K. Effect of aluminum content on the passivation behavior of Fe–Al alloys in sulfuric acid solution. *J. Mater. Sci.* **2006**, *41*, 3041–3044. [CrossRef]
19. Sharma, G.; Singh, P.R.; Sharma, R.K.; Gaonkar, K.B.; Ramanujan, R.V. Aqueous corrosion behavior of iron aluminide intermetallics. *J. Mater. Eng. Perform.* **2007**, *16*, 779–783. [CrossRef]
20. Porcayo-Calderon, J.; Luna, A.; Arrieta-Gonzalez, C.D.; Salinas-Bravo, V.M. Corrosion performance of Fe-Al intermetallic coatings in 1.0 M NaOH solution. *Int. J. Electrochem. Sci.* **2013**, *8*, 12205–12218.
21. Ji, G.; Elkedim, O.; Grosdidier, T. Deposition and corrosion resistance of HVOF sprayed nanocrystalline iron aluminide coatings. *Surf. Coat. Technol.* **2005**, *190*, 406–416. [CrossRef]
22. Liu, T.; Lau, K.-T.; Chen, S.; Cheng, S.; He, T.; Yin, Y. The electrochemistry corrosion behavior of Fe_3Al-type intermetallic with super-hydrophobic surfaces. *Mater. Manuf. Process.* **2010**, *25*, 298–301. [CrossRef]
23. Rao, V.S. Repassivation behaviour and surface analysis of Fe_3Al based iron aluminide in 0.25 M H_2SO_4. *Corros. Sci.* **2005**, *47*, 183–194.
24. Huape-Padilla, E.; Sanchez-Carrillo, M.; Flores-De los Ríos, J.P.; Espinosa-Medina, M.J.; Raúl Germán, B.M.; Ferrer-Sánchez, M.I.; Carbajal-de-la-Torre, G.; Bejar-Gómez, L.; Chacon-Nava, J.; Martinez-Villafane, A. Corrosion study of Fe-Al intermetallic alloys in simulated acid rain. *Int. J. Electrochem. Sci.* **2015**, *10*, 2141–2154.
25. Amiriyan, M.; Blais, C.; Savoie, S.; Schulz, R.; Gariepy, M.; Alamdari, H. Mechanical behavior and sliding wear studies on iron aluminide coatings reinforced with titanium carbide. *Metals* **2017**, *7*, 177. [CrossRef]
26. Rosalbino, F.; Carlini, R.; Parodi, R.; Zanicchi, G.; Scavino, G. Investigation of passivity and its breakdown on Fe_3Al–Si and Fe_3Al–Ge intermetallics in chloride-containing solution. *Corros. Sci.* **2014**, *85*, 394–400. [CrossRef]
27. Negache, M.; Taibi, K.; Souami, N.; Bouchemel, H.; Belkada, R. Effect of Cr, Nb and Zr additions on the aqueous corrosion behavior of iron-aluminide. *Intermetallics* **2013**, *36*, 73–80. [CrossRef]
28. Rosalbino, F.; Carlini, R.; Zanicchi, G.; Scavino, G. Effect of copper alloying addition on the electrochemical corrosion behavior of Fe_3Al intermetallic in sulphuric acid solution. *Mater. Corros.* **2016**, *67*, 1042–1048. [CrossRef]
29. Zamanzade, M.; Vehoff, H.; Barnoush, A. Cr effect on hydrogen embrittlement of Fe_3Al-based iron aluminide intermetallics: Surface or bulk effect. *Acta Mater.* **2014**, *69*, 210–223. [CrossRef]
30. Rao, V.S.; Baligidad, R.; Raja, V. Effect of carbon on corrosion behavior of Fe_3Al intermetallics in 0.5 N sulphuric acid. *Corros. Sci.* **2002**, *44*, 521–533. [CrossRef]

31. McKamey, C.; Horton, J.; Liu, C. Effect of chromium on properties of Fe_3Al. *J. Mater. Res.* **1989**, *4*, 1156–1163. [CrossRef]
32. Keddam, M.; Mattos, O.R.; Takenouti, H. Mechanism of anodic dissolution of iron-chromium alloys investigated by electrode impedances—I. Experimental results and reaction model. *Electrochim. Acta* **1986**, *31*, 1147–1158. [CrossRef]
33. Keddam, M.; Mattos, O.; Takenouti, H. Mechanism of anodic dissolution of iron-chromium alloys investigated by electrode impedances—II. Elaboration of the reaction model. *Electrochim. Acta* **1986**, *31*, 1159–1165. [CrossRef]
34. Epelboin, I.; Keddam, M.; Mattos, O.R.; Takenouti, H. The dissolution and passivation of Fe and FeCr alloys in acidified sulphate medium: Influences of pH and Cr content. *Corros. Sci.* **1979**, *19*, 1105–1112. [CrossRef]
35. Zamanzade, M.; Barnoush, A. An overview of the hydrogen embrittlement of iron aluminides. *Procedia Mater. Sci.* **2014**, *3*, 2016–2023. [CrossRef]
36. Arrieta-Gonzalez, C.; Porcayo-Calderon, J.; Salinas-Bravo, V.; Gonzalez-Rodriguez, J.; Chacon-Nava, J. Electrochemical behavior of Fe_3Al modified with Ni in Hank's solution. *Int. J. Electrochem. Sci.* **2011**, *6*, 4016–4031.
37. Osório, W.R.; Freitas, E.S.; Garcia, A. EIS and potentiodynamic polarization studies on immiscible monotectic Al–In alloys. *Electrochim. Acta* **2013**, *102*, 436–445. [CrossRef]
38. Devos, O.; Gabrielli, C.; Tribollet, B. Simultaneous EIS and in situ microscope observation on a partially blocked electrode application to scale electrodeposition. *Electrochim. Acta* **2006**, *51*, 1413–1422. [CrossRef]
39. Jorcin, J.-B.; Mark, M.O.; Nadine, P.; Bernard, T. CPE analysis by local electrochemical impedance spectroscopy. *Electrochim. Acta* **2006**, *51*, 1473–1479. [CrossRef]
40. Zamanzade, M.; Barnoush, A. Effect of chromium on the electrochemical properties of iron aluminide intermetallics. *Corros. Sci.* **2014**, *78*, 223–232. [CrossRef]